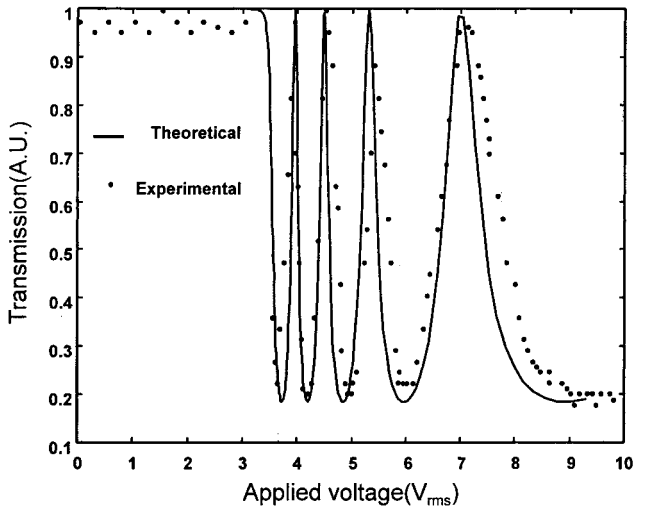

Figure 5 Both calculated and measured results for the LC-FPIs

tively. These two cases show almost the same behaviors: the pattern contrast is high and the rings result purely from the extraordinary component λ_e.

The β-dependence of the extinction ratio for these two structures was measured by rotating the transmitted axis of the polarizer in front of the LC-FPI, as shown in Figure 4. The extinction ratio of the single-LC-layer structure decreases as β increases, and becomes zero at $\beta = 90°$. The zero extinction ratio appears at $\beta = 90°$ because the propagating light only encounters the ordinary refractive index of the LC director, no matter how much we change the tuning voltage. At the same time, the extinction ratio of our proposed double-LC-layer structure almost remains constant (= 7.4 dB) at different β angles. This further elucidates the fact that this structure is polarization-independent.

In our proposed structure, the double-LC-layer LC-FPI, two layers of LC films and one layer of glass substrate between the two mirrors form a resonant cavity, thus it is very important to obtain the voltage-dependence of the transmission. Figure 5 shows this dependence for both simulated and measured results. If a large resonant cavity length is required for certain applications with small FWHM, this double LC-layer LC-FPI is appropriate, because the middle glass substrate will enlarge the cavity length rather than increase the thickness of LC layer. Moreover, the two layers of the LC are simultaneously but separately driven by the voltage source, so that the response time of this device will not be sacrificed.

CONCLUSION

As discussed in this paper, the proposed double-layer LC-FPI shows good performance with regards to polarization-independence, extinction ratio, voltage-dependence of transmission, response time, and even FWHM. By using this novel and easy-to-fabricate structure, we can obtain the entirely pure resonant wavelength, say, the extraordinary component λ_e, without mixing with the ordinary component λ_o. The fluctuations of polarization-dependent power were demonstrated at less than 0.5 dB and the extinction ratios at up to 7 dB.

REFERENCES

1. H. Yoda, Y. Ohtera, O. Hanaizumi, and S. Kawakami, Analysis of polarization-insensitive tunable optical filter using liquid crystal: Connection formula and apparent paradox. Optical and Quantum Electronics 29 (1997), 285–299.
2. J.S. Patel and M.W. Maeda, Tunable polarization diversity liquid-crystal wavelength filter, IEEE Photonics Tech Lett 3 (1991), 739–740.
3. J.S. Patel and M.W. Maeda, Multiwavelength tunable liquid-crystal etalon filter, IEEE Photon Technol Lett 3 (1991), 643–644.
4. J.S. Patel and S.D. Lee, Electrically tunable and polarization insensitive Fabry–Perot etalon with a liquid-crystal film, Appl Phys Lett 58 (1991), 2491–2493.
5. K. Hirabayashi, Y. Ohiso, and T. Kurokawa, Polarization-independent tunable wavelength-selective filter using a liquid crystal, IEEE Photon Technol Lett 3 (1991), 1091–1093.
6. K. Hirabayashi and T. Kurokawa, A tunable polarization-independent liquid-crystal Fabry–Perot interferometer filter, IEEE Photon Technol Lett 4 (1992), 740–742.
7. P.L. Chen, K.C. Lin, W.C. Chuang, Y.C. Tzeng, K.Y. Lee, and W.Y. Lee, Analysis of a liquid crystal Fabry–Perot etalon filter: A novel model, IEEE Photon Technol Lett 9 (1997), 467–469.

A 5.8-GHz LNA WITH IMAGE REJECTION AND GAIN CONTROL BASED ON 0.18-μm CMOS

Jin-pil Kim,[1] Yong-Hun Oh,[1] Jin-Young Choi,[2] and Sang-gug Lee[1]
[1] School of Engineering,
Information and Communications University 58-4
Hwaam-dong, Yuseong-gu
Daejon, 305-732, Korea
[2] School of Electrical, Electronic, and Computer Engineering
Hongik University
Jochiwon, Chungnam, 339-701, Korea

Received 26 February 2003

ABSTRACT: *This paper presents a low-noise amplifier (LNA) design which includes image rejection and gain control. The proposed LNA adopts a cascode topology with a notch filter combined with a gain control function. The performance of the proposed LNA is compared with conventional cascode topology and improvements in noise figure and image rejection by 0.3 and 11.5 dB, respectively, are confirmed. The proposed 5.8-GHz LNA is implemented using 0.18-μm CMOS technology. Measured high-gain mode performances show noise figure (NF) = 1.4 dB, gain = 16.5 dB, and input-$P_{1dB} = -8$ dBm; with low-gain mode, the gain reduces to 5.5 dB while the linearity improves to input-$P_{1dB} = 10$ dBm. The LNA dissipates 4 mA from a 1.8 V supply.* © 2003 Wiley Periodicals, Inc. Microwave Opt Technol Lett 38: 477–480, 2003; Published online in Wiley InterScience (www.interscience.wiley.com). DOI 10.1002/mop.11094

Key words: *low noise amplifier; RF; cascode; image rejection; gain control*

1. INTRODUCTION

Due to its excellent sensitivity and selectivity, the superheterodyne architecture is the most widely used receiver topology in modern wireless communication systems. One of the issues related to superheterodyne receivers is image. Generally, off-chip passive filters such as surface acoustic wave (SAW) or ceramic filters are used for image rejection. These external filters, which cannot be easily integrated, are the major impediment to raising the integration level of radio frequency (RF) circuits. In addition, the external filters tend to be expensive and large in size. Some monolithic solutions to this issue have been proposed. For frequencies below 3 GHz, monolithic image reject mixers with more than 40 dB of image rejection have been reported [1–3]. However, due to the

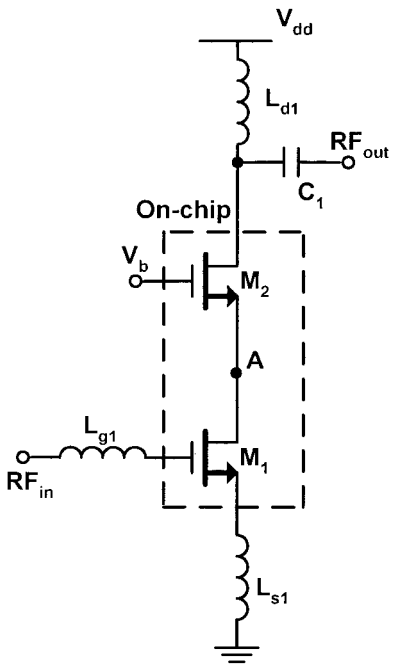

(a)

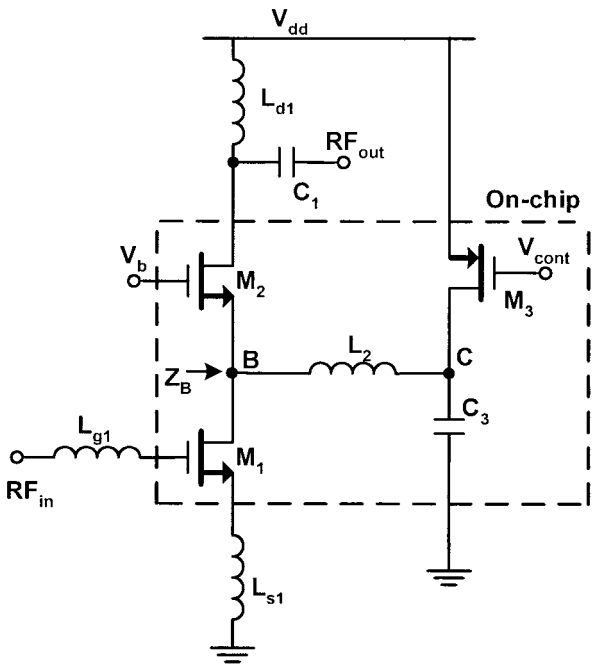

(b)

Figure 1 LNA schematics: (a) conventional cascode and (b) proposed topology

gain and phase mismatches, which correspond to a time mismatch of under 0.6 ps, the image-rejection ratios for 5-GHz band receivers generally lie within the range of 25–35 dB [4]. Practical systems require higher amounts of image rejection. Therefore, by combining an on-chip image-rejection filter with an integrated image-rejection mixer, acceptable image rejection can be obtained. The LNA proposed in this work can be used as a matching pair to the image-rejection mixer.

The variation of LNA gain is an efficient way to improve the dynamic range of the receiver. In the presence of small incoming

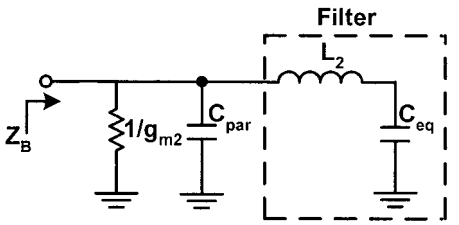

Figure 2 Simplified small-signal equivalent circuit looking into node B in Fig. 1(b)

signals, the LNA operates with maximum gain and minimum noise figure (NF). Hence, with strong signals, the LNA can be switched into low-gain mode and provide higher linearity.

The proposed LNA adopts gain control into the image-rejection circuit, which makes the LNA quite desirable. The image-rejection circuit also helps to reduce the noise contribution of the LNA core's cascode transistor. In section 2, the details of LNA design are described. The measurement results are described in section 3 and section 4 concludes this paper.

2. LNA DESIGN

Figure 1 shows two LNA topologies: (i) conventional cascode and (ii) proposed cascode. In Figure 1, the input and output matching components L_{g1}, L_{s1}, L_{d1}, and C_1 are added as off-chip elements. As expected, the size of L_{s1} is selected for simultaneous matching of gain and noise [5] (Fig. 1). To minimize NF degradation by the resistance in the inductor at the input, L_{s1} is implemented with bond wire.

Using the conventional cascode LNA topology presented in Figure 1(a), the noise contribution of M_2 can be significant at high frequencies due to the parasitic capacitances at node A. The idea of adding a filter at node A has been proposed as a way to resolve the NF degradation as well as to provide image-rejection capability [4]. The proposed LNA topology shown in Figure 1(b) adopts the same idea, but modifies it to accommodate the gain control current source M_3. In Figure 1(b), the size of L_2 and C_3 are selected to resonate serially at the image frequency; at the same time, the size of L_2 is chosen for parallel resonance with the parasitic capacitance at node B. The spiral inductor L_2 and the MIM capacitor C_3 are implemented as on-chip elements. In order to obtain a higher quality (Q) factor, the spiral inductor has been implemented with a thick metal top layer. In Figure 1(b), the series resonance at image frequency suppresses the image signal from appearing at the output, while the parallel resonance provides high impedance at

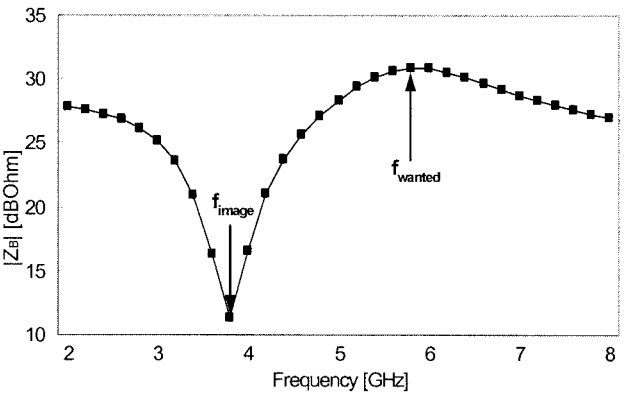

Figure 3 Impedance Z_B looking into node B in Fig. 1(b)

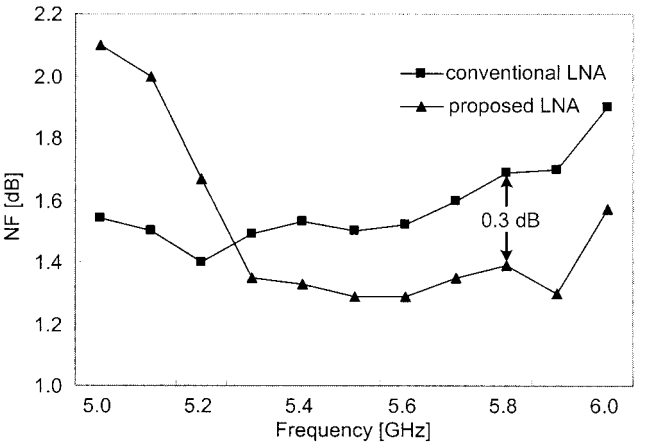

Figure 4 Measured NF vs. frequency of conventional and proposed LNAs

the source of the cascode transistor M_2, such that the noise contribution of M_2 at the output can be reduced.

Figure 2 represents the simplified small-signal equivalent circuit looking into node B in Figure 1(b). In Figure 2, C_{par} represents the parasitic capacitances at the drain and source of M_1 and M_2 (node B), respectively, C_{eq} is the sum of C_3 and the parasitic capacitance at node C, and g_{m2} is the transconductance of transistor M_2.

From Figure 2, the impedance Z_B can be given by

$$Z_B(s) = \frac{s^2 L_2 C_{eq} + 1}{s(s^2 C_{par} L_2 C_{eq} + C_{par} + C_{eq})}. \quad (1)$$

From Eq. (1), it can be seen that the filter has imaginary zeros and poles at

$$f_{image} = \frac{1}{2\pi\sqrt{L_2 C_{eq}}} \quad (2)$$

and

$$f_{wanted} = \frac{1}{2\pi}\sqrt{\frac{1}{L_2}\left(\frac{1}{C_{par}} + \frac{1}{C_{eq}}\right)}, \quad (3)$$

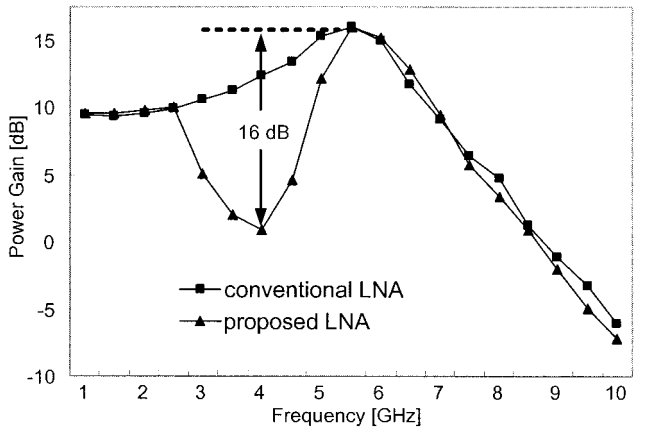

Figure 5 Measured power gain vs. frequency of conventional and proposed LNAs

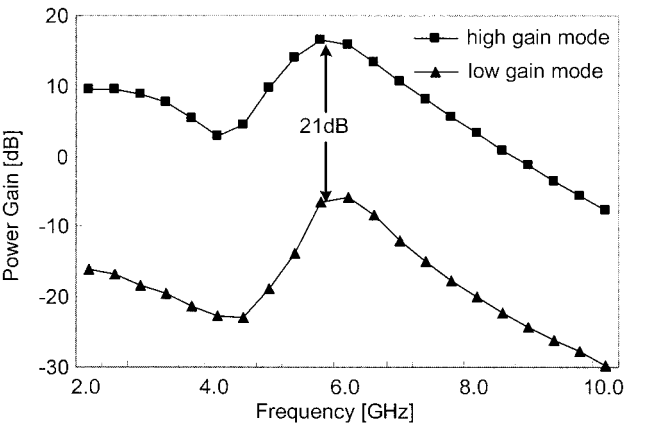

Figure 6 Measured power gain of the proposed LNA under low- and high-gain modes

where f_{image} and f_{wanted} are the frequencies of the image and wanted signal, respectively. From Eqs. (2) and (3), the values of f_{image} and f_{wanted} can be selected simultaneously by the proper selection of L_2 and C_3.

Figure 3 shows the frequency behavior of the impedance Z_B looking into the node B in Figure 1(b), based on simulations. As can be seen in Figure 3, the image-rejection filter provides a deep notch at f_{image} and the non-peaky behavior of the parallel-resonated impedance at f_{wanted} is due to $1/g_{m2}$. However, note that the resonated impedance seen by the common-gate transistor M_2, which is critical in order to minimize the noise contribution of transistor M_2, is not affected by $1/g_{m2}$.

As previously described, the proposed LNA shown in Figure 1(b) combines gain controllability with the series-parallel filter. With a small input signal, the gain-control transistor M_3 would remain off. In this high-gain condition, the gain-control transistor contributes no noise signal to the LNA, except the parasitic capacitance. However, with an input signal above a certain level, the control voltage can be set to such a low amount that the common-gate transistor M_2 would turn off. In the low-gain mode, the noise contribution of transistor M_3 is no longer an issue and the common-source part of the cascode amplifier operates with nearly the same amount of linearity as in the case of the high-gain mode. However, the common-gate part operates as a passive attenuator, contributing no additional distortion to the LNA. Therefore, the input-referred linearity of the amplifier is expected to be improved roughly by the amount of reduced gain, leading to larger overall dynamic range of a receiver.

3. MEASUREMENT RESULTS

In this work, in order to exploit the advantage of the proposed LNA, both conventional and proposed LNAs, as shown in Figure

TABLE 1 Summary of the Measured LNA Performances

Performances	Proposed LNA		Conventional LNA
	High-Gain Mode	Low-Gain Mode	
Frequency of operation (GHz)	5.8	5.8	5.8
Power consumption with V_{DD} = 1.8 V (mW)	7.2	7.2	7.2
Noise figure (dB)	1.39	—	1.69
Power gain (dB)	16.5	−5.5	16.5
Input-P_{1dB} (dBm)	−8	10	−8
Image rejection (dB)	16		4.5

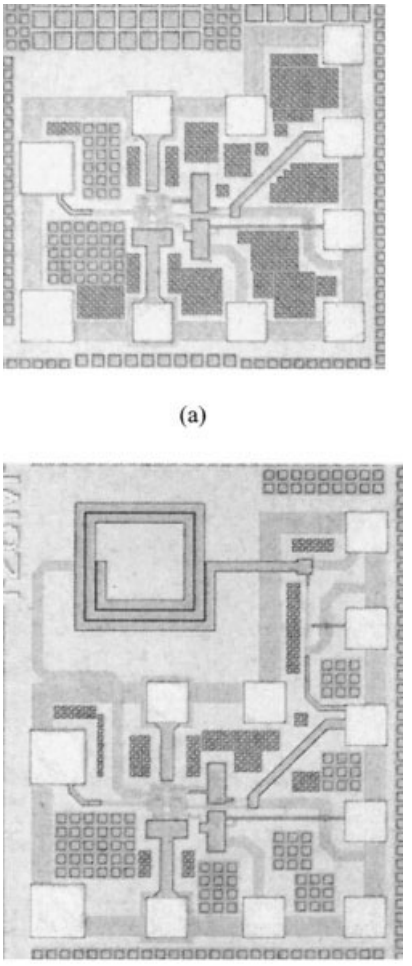

Figure 7 Microphotograph of (a) conventional and (b) proposed LNAs

1, are fabricated based on a 0.18-μm CMOS technology. The LNAs are optimized for 5.8-GHz wireless LAN applications and biased to dissipate 4 mA from a 1.8-V supply.

Figure 4 shows the measured NF versus the frequency of the LNAs. As can be seen from the figure, the proposed LNA presents high NF near the image frequency, due to the signal loss through the notch filter. However, as the frequency approaches 5.8 GHz, the noise figure is reduced to lower than that of the conventional cascode LNA. This confirms that the adopted filter provides higher impedance to the source of the common-gate transistor M_2 shown in Figure 1(b). At 5.8 GHz, the proposed LNA shows a 0.3-dB improvement in NF as compared to the conventional LNA.

Figure 5 shows the power gain of the two LNAs. As can be seen from the figure, the image-rejection filter provides approximately 16 dB of overall image rejection. Both LNAs provide 16.5 dB of power gain at 5.8 GHz.

Figure 6 shows the measured power gain of the proposed LNA in its high- and low-gain modes. The LNA gain varies by the amount of 21 dB (Fig. 6). At the frequency of interest, 5.8 GHz, the power gains at high- and low-gain modes are 16.5 and -5.5 dB, respectively. The corresponding input 1-dB compression points are -8 and 10 dBm, respectively, which indicates 18 dB of improvement in linearity under low-gain mode. Table 1 summarizes the measurement results and Figure 7 shows a microphotograph of the two LNAs.

4. CONCLUSION

In this paper, an LNA that can suppress the image signal and control the amount of gain is proposed. The proposed LNA is implemented using 0.18-μm CMOS technology and compared with conventional topology. The measurement results show that the addition of image-rejection and gain-control circuits leads to an overall image rejection of 16 dB and 21-dB gain variation. The NF of the proposed LNA improves by 0.3 dB in its high-gain mode and the linearity improves by 18 dB in its low-gain mode. In its high-gain mode, the proposed LNA shows a noise figure of 1.4 dB, power gain of 16.5 dB, and input-P_{1dB} of -8 dBm, while dissipating 4 mA from a 1.8-V supply.

REFERENCES

1. P.B. Khannur, and K.S. Ling, A 2.45GHz fully-differential CMOS image-reject mixer for Bluetooth application, IEEE MTT-S Dig (2002), 549–552.
2. F. Behbahani et al., An adaptive 2.4GHz low-IF receiver in 0.6μm CMOS for wideband wireless LAN, IEEE ISSCC, 2000, pp. 146–147.
3. M. Ugajin et al., A 1V 12mW 2GHz receiver with 49dB image rejection in CMOS/SIMOX, IEEE ISSCC, 2001, pp. 288–289.
4. T.H. Lee, H. Samavati, and H.R. Rategh, 5-GHz CMOS wireless LANs, IEEE Trans Microwave Theory Techn 50 (2002), 268–280.
5. K.O., Estimation methods for quality factors of inductors fabricated in silicon integrated circuit process technologies, IEEE J Solid-State Circ 33 (1998), 1249–1252.

CHARACTERISTICS OF GAUSSIAN PULSES TRANSMITTING IN THE G.652 FIBER WITH FBG DISPERSION COMPENSATION

Li Pei, Shuisheng Jian, Fengping Yan, Tangjun Li, and Tigang Ning
Institute of Light-wave Technology
Northern Jiaotong University
Beijing, 100044, P. R. China

Received 27 February 2003

ABSTRACT: *The compression characteristics of a Gaussian pulse with varied chirp and pulse width are obtained by theoretical analysis and experiments. The compensation effects are diverse, even with the same chirped optical fiber Bragg grating (FBG) dispersion compensator, and the optimal dispersion compensation length is related to the position of the FBG. At present, in most of transmission systems, the signal from the lasers are Gaussian pulses, thus an analysis of its broader characteristics, before and after it is reflected from the FBG, will be significant.* © 2003 Wiley Periodicals, Inc.
Microwave Opt Technol Lett 38: 480–484, 2003; Published online in Wiley InterScience (www.interscience.wiley.com). DOI 10.1002/mop.11095

Key words: *Gaussian pulses; high speed, long-haul optical communication; FBG; dispersion compensation*

1. INTRODUCTION

Because of its huge communication capacity and inexpensive building outlay, optical-fiber communications technology provides an infinite broadband communication platform and thus the all-